RSC Advances

PAPER

View Article Online
View Journal | View Issue

Cite this: *RSC Adv.*, 2023, **13**, 7514

Sustainable product-based approach in the production of olefins using a dual functional ZSM-5 catalyst

Mohsen Rostami Sakha,[a] Parya Halimitabrizi,[ab] Saeed Soltanali, *[c] Fatemeh Ektefa,[c] Zeinab Hajjar[d] and Dariush Salari[a]

Received 3rd January 2023
Accepted 27th February 2023

DOI: 10.1039/d3ra00037k

rsc.li/rsc-advances

Investigation of the current industrial processes, such as methanol to olefin (MTO) and hexane to olefin (HTO), in terms of green and sustainable chemistry approaches in order to design the process, catalyst and reactor from the beginning in such a way as to minimize environmental pollution is compulsory. Therefore, the synthesis of a group of multifunctional catalysts, which can be used simultaneously in both industrial processes to produce a variety of products, was studied. The effect of incorporation of different metals (Fe, Mn, Zn, Ga and Al) on the strengthening of each of the products was also studied. The investigation of reactor productivity ($WHSV_{HTO} = 25$) in HTO showed that the production efficiency of propylene in microchannels is higher than the ideal value for all samples, which is a significant improvement for sustainable approaches in future technologies. Considering the overall performances, Ga-ZM showed the best performance in both processes due to the high *P*/*E* ratio. The significant effect of Ga on the increasing of propylene was confirmed in MTO at 400 °C ($P/E \simeq \infty$), which indicated the dramatic effect of this metal in directing the reaction mechanism to an olefin-based cycle by converting almost all ethylene to propylene by methylation.

1. Introduction

Light olefins, which form more than 60% of the total production of the petrochemical industry (400 million tonnes), are considered the most important basic building blocks of various chemical products from polymers to pharmaceutical compounds.[1–4] Traditional processes such as ethane/propane cracking and other processes such as methanol to olefin conversion (MTO) and naphtha cracking (hexane, as model compound, to olefin (HTO)) have become a threat to the environment despite the production of desirable products; especially propylene, due to the generation of solid and liquid wastes, high energy consumption, low *P*/*E* ratio and emission of greenhouse gases; especially methane, as the second most important greenhouse gas.[5–9] It is the time to adopt alternative routes to reduce the consumption and production of waste and toxic compounds from their inception to prevent environmental pollution, due to the enormous value of the chemical industry. Therefore, for the production and processing of light olefins, the needs for novel catalysts and processes, enhanced energy efficiency and identification of renewable feedstocks are felt.[10–12] According to the metrics of sustainable performance, environmental pollution in catalytic processes can be minimized whenever the criteria of waste production, selectivity, reactor productivity (RP), product concentration, and catalyst consumption (CC) prevail during the catalytic process.[13] Otherwise, the implementation of a catalytic process, even if the desirable products are formed, is not environmentally friendly and will lead to pollution.[14]

By synthesizing catalysts, which can perform optimally in several reactions (multifunctional catalysts) and performing the processes under milder conditions by modern technologies, propylene can be produced by both MTO and naphtha cracking processes through a sustainable approach.[15] Zeolites with different topologies, acidic properties and morphologies facilitate the production of desirable products based on the type of reactants and the operating conditions in various processes. In fact, the framework of zeolites can be optimized based on the purpose.[16–18] Meanwhile, ZSM-5 zeolite with microporous structure is a versatile catalyst with a great impact on catalytic applications due to its shape selectivity. It should be noted that ZSM-5 typically suffers from simple microporous structure, long diffusion paths, and strong additional acid sites, which ultimately leads to low catalytic activity in both MTO and HTO processes.[19–21] Improving the proper methods of ZSM-5 synthesis makes it possible to overcome the limitations while

[a]*Reactor and Catalysis Research Lab., Department of Chemistry, University of Tabriz, Iran*
[b]*Department of Chemical and Petroleum Engineering, University of Tabriz, Iran*
[c]*Catalysis Technologies Development Division, Research Institute of Petroleum Industry (RIPI), Tehran, Iran. E-mail: soltanalis@ripi.ir; sssoltan@gmail.com*
[d]*Nanotechnology Research Division, Research Institute of Petroleum Industry (RIPI), Tehran, Iran*

maintaining its ability to produce the desired products. In other words, proper synthesis allows the growth of nanoscale crystal structures, hierarchically with different pore types without using additional chemicals.[22,23] Simultaneously, the limitations preventing the using of ZSM-5 in both MTO and HTO processes can be minimized by altering the acidic properties.[24,25] Changing the pore structure and acidity of ZSM-5 enhances its catalytic activity and selectivity to light olefins, making it a key catalyst in the chemical industry. ZSM-5 catalysts can achieve the goals of green chemistry when the desired structural properties are formed by using environmentally friendly conditions and compound in addition to increasing the production of the desired product.

Generally, catalytic reactions are limited due to the poor heat and mass transfer performance; therefore, the catalyst efficiency and lifetime are minimized. The high surface area-to-volume (SAV) ratio (typically about 10–100 times more than conventional reactors) in microchannel reactors enhance the catalyst efficiency in comparison with fixed- and fluidized-bed reactors. The correction of temperature fluctuations in microchannels, which prevents the formation of hot spots along the catalytic bed during exothermic processes as well as enhancing the proper conduction of heat along the catalytic bed during the endothermic processes, is immediately possible. Microchannel technology is a modern approach, which minimizes the negative environmental impacts on a wide range of chemical products. According to the principles of green chemistry, microchannels can play an essential role in achieving sustainable catalytic processes.[26–31]

In the present study, for the first time, sustainable chemistry approaches based on the metrics recently proposed by Shell have been given first priority. Therefore, the feed flow was increased compared to the two recent reports by this group to investigate the effect of various incorporated metals in MTO and HTO processes, using microchannels. Additionally, the effect of temperature was studied in MTO to reduce energy consumption in the performance of incorporated zeolites. The synthesized zeolites were obtained under milder conditions (less template consumption, lower crystallization temperature, using non-templating method to achieve hierarchical zeolites, and less crystallization time) compared to our previous works in order to obtain cleaner products in terms of green and sustainable chemistry. Furthermore, the effect of metal substitution on the textural and acidic properties as well as the performance in two industrial processes in order to achieve multifunctional catalysts was studied.

2. Experimental

2.1. Catalyst preparation

Zeolites were obtained by sol–gel method using aluminum sulphate ($Al_2(SO_4)_3 \cdot 18H_2O$, Merck Chemical Co.) and Colloidal Silica (40 wt% SiO_2, Aldrich Chemical Co.) as Al and Si sources, respectively. The molar composition of the synthesized zeolites was $100SiO_2$: $0.125Al_2O_3$: $0.125M_2O_3$: 0.1TPAOH: $0.19Na_2O$: $0.205NH_4F$: $32H_2O$ (M = Fe, Mn, Zn, Ga and Al) and Si/(Al + M) = 200 for all samples. The zeolites were crystalized dynamically at 160 °C for 40 h followed by drying and calcination in the temperature range of 120–550 °C for 14 h to avoid forming defects and large crystals. H-ZSM-5 was obtained by ion-exchanging the powder with NH_4NO_3 (1 M) at 80 °C two times, followed by calcination at 600 °C following the same temperature programming.

2.2. Characterization

An Inel EQUINOX 3000 X-ray diffractometer with Cu Kα radiation at 40 kV and 100 mA was used to obtain XRD (X-ray diffraction) patterns in the 2θ = 7–60° range with a step size of 0.02°. A Zeiss Sigma VP field emission scanning electron microscope (FE-SEM) was used to acquire SEM (Scanning Electron Microscopy) images and EDX (Energy Dispersive X-ray analysis) maps. The N_2 adsorption–desorption isotherms, surface areas and pore volumes were obtained at −196 °C using a Micromeritics instrument after evacuation for 7 h. NH_3 temperature-programmed desorption (NH_3-TPD) and H_2 temperature-programmed reduction (H_2-TPR) were carried out on a Micromeritics TPR/TPD 2900 chemisorption analyzer. Inductively coupled plasma-optical emission spectroscopy (ICP-OES) analysis was employed to determine the percentage of metals in the composite using a Varian VISTA-PRO analyzer. A Bruker Vertex80 spectrophotometer was used to record the FTIR (Fourier transform infrared) spectra of the synthesized catalysts in the 400–4000 cm^{-1} range. UV-Visible Diffuse Reflectance Spectra (UV-Vis DRS) analysis of synthesized sample was recorded on Shimadzu UV-2600i spectrophotometer at room temperature and ambient atmosphere. Since its wavelength range can easily be expanded to the near-infrared region of 1400 nm using the optional integrating sphere the wavelength was set in the absorption range of 190 to 1100.

2.3. Catalytic performance

The performance of the synthesized catalysts was evaluated in the catalytic cracking of *n*-hexane (naphtha model feed) and methanol to olefin reactions. A 5-channel microreactor, each channel with dimensions of 50 × 1 × 1 mm, was operated to perform the catalytic tests. Catalytic cracking of *n*-hexane was performed at 600 °C and atmospheric pressure under N_2 flow as the carrier gas. The catalyst was initially activated *in situ* by heating at 550 °C for 2 h in a 30 mL min^{-1} N_2 flow. MTO was investigated at 450 and 400 °C to study the effect of temperature. The activation step in MTO was the same except the temperature which was reduced to 500 °C. 0.125 g of meshed zeolite (sieve fraction 150–250 μm) was packed in the microchannels in each of the reactions. The outlet gas was analyzed every 2 hours. The products were analyzed by an online gas chromatograph (Shimadzu 2010 Plus GC) equipped with a flame ionization detector (FID) with HP-PLOT Al_2O_3 capillary column.

2.4. Catalytic performance calculations based on the sustainable metrics

The data for the sustainable metrics were obtained from the following calculations:

$$\text{Catalyst consumption} = \text{kg}_{\text{cat}}/\text{tonnage}_{\text{product}}$$

$$\text{Rector productivity} = \frac{\text{tonnage}_{\text{product}}}{\text{reacto volume}_{\text{m}^3} \times \text{reaction}_{\text{time}}}$$

RH = required hours of stability to decrease the catalyst consumption to the ideal value.

3. Results and discussion

3.1. Structural, textural and acidic properties

Fig. 1 demonstrates the XRD patterns of ZSM-5 zeolites incorporated with various metals. The formation of uniform nanocrystals is clear in the corresponding pattern due to the clear distinctions in the peak range of 21–27°. A closer investigation of the peaks above $2\theta = 25°$ shows the absence of the peaks related to the metal oxides, which proves the symmetrical distribution and/or incorporation of metals into the structure of zeolites.

The SEM images (Fig. 2) of the incorporated zeolites illustrated the formation of uniform nanocrystals (<100 nm) due to optimal synthesis conditions and fluoride environment. In addition, all zeolites, except Zn-ZM, demonstrated almost the same particle size due to the low amounts of substituted metals. Furthermore, the lack of extra-structural species was proved by the surface clarity of the formed particles, which was in line with the XRD profiles. The compounds used in the synthesis as well as the operated synthesis method in the preparation of the catalysts, which were incorporated with the various metals, showed no accumulation of elements and a significantly uniform distribution of the elements in the mapping images (Fig. 3), which also confirmed the incorporation of metals into the structure and/or uniform dispersion in the cavities and surfaces of catalysts.[31,32]

Fig. 4 shows the N_2 adsorption–desorption isotherms of BET for the incorporated zeolites. The formation of type IV isotherm was quite evident in the study of the relevant isotherms, which indicated the formation of mesopores in zeolites incorporated with different metals. Mesoporous structures enhance the transfer of products from the catalytic bed and ultimately increase their activity and stability. The obtained pore size distribution profiles (Fig. 5) also showed that all samples had pores in the range of 1–6 nm, which indicated the formation of narrow mesopore structures and super-uniform nanocrystals. All the incorporated catalysts showed a combination of types H_2, H_3 and H_4 hysteresis loops due to a sharp increase of the slope in the range of $P/P_0 > 0.4$, with capillary condensation. This combination indicated the formation of interconnected mesopores, which confirmed the homogeneous nanocrystalline

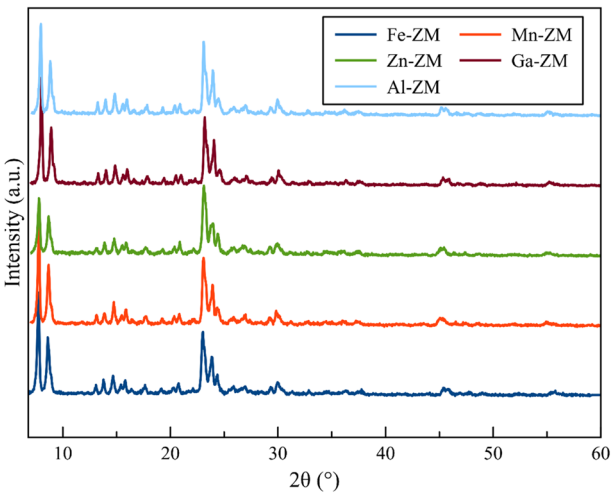

Fig. 1 XRD patterns of incorporated zeolites.

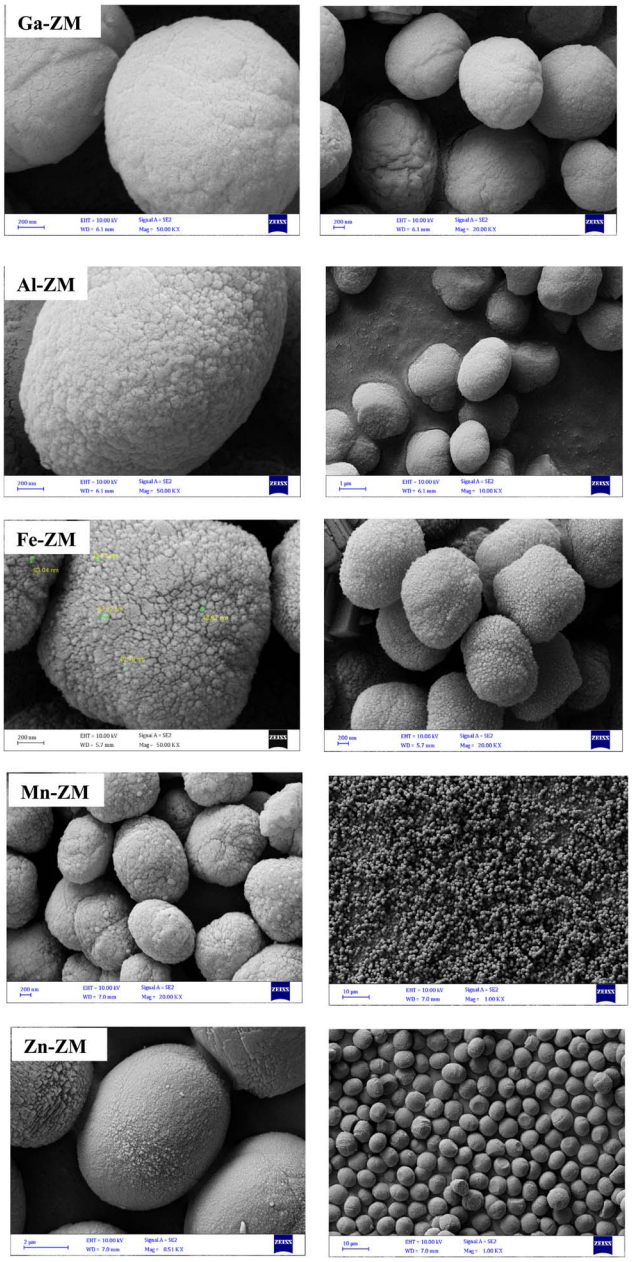

Fig. 2 FE-SEM images of zeolites.

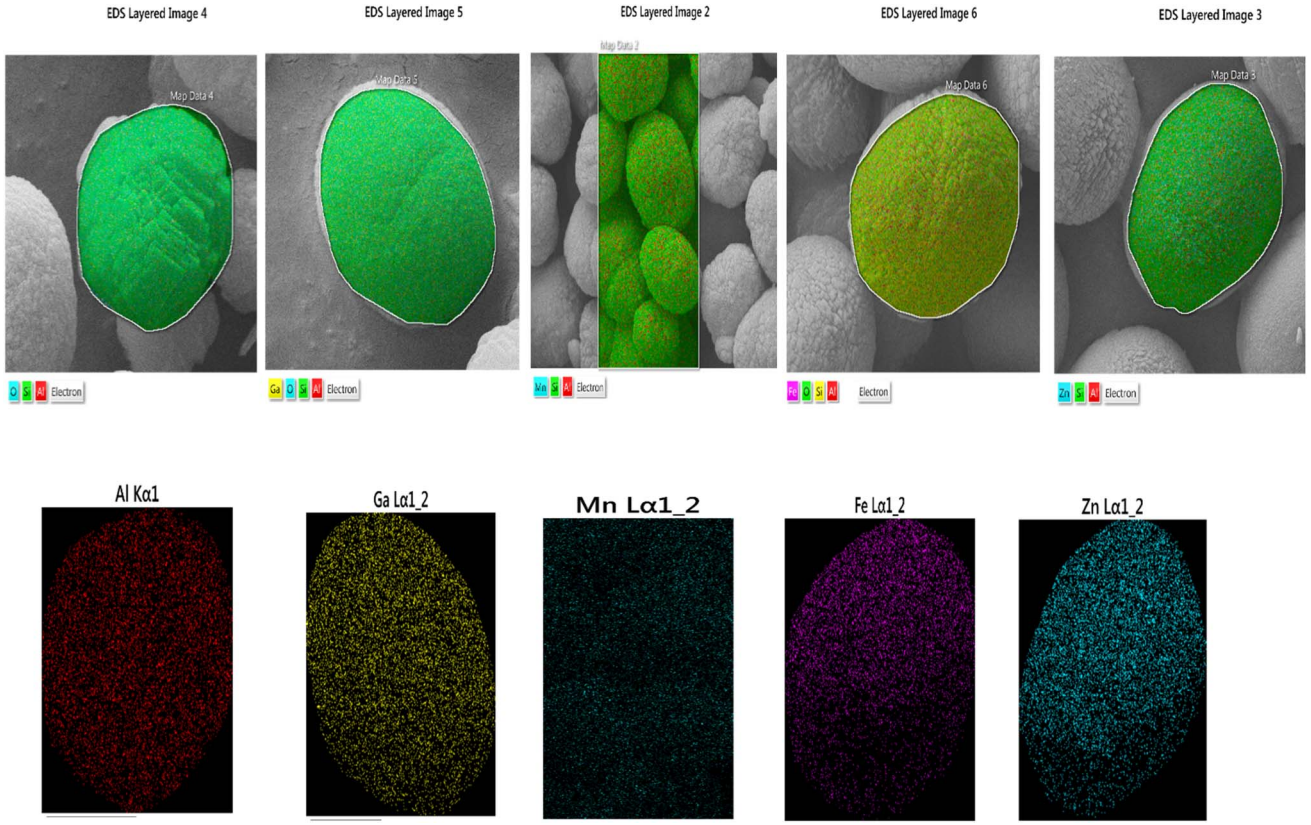

Fig. 3 EDX maps of zeolites.

structures in SEM images. In addition, the hysteresis loop in the range of $P/P_0 > 0.9$ indicated the presence of wider and larger mesopores in all samples, which was carefully in line with pore size distribution curves. According to Table 1, high external surface area was also formed in all samples, which is in agreement with the formation of mesoporous structures.[33–35]

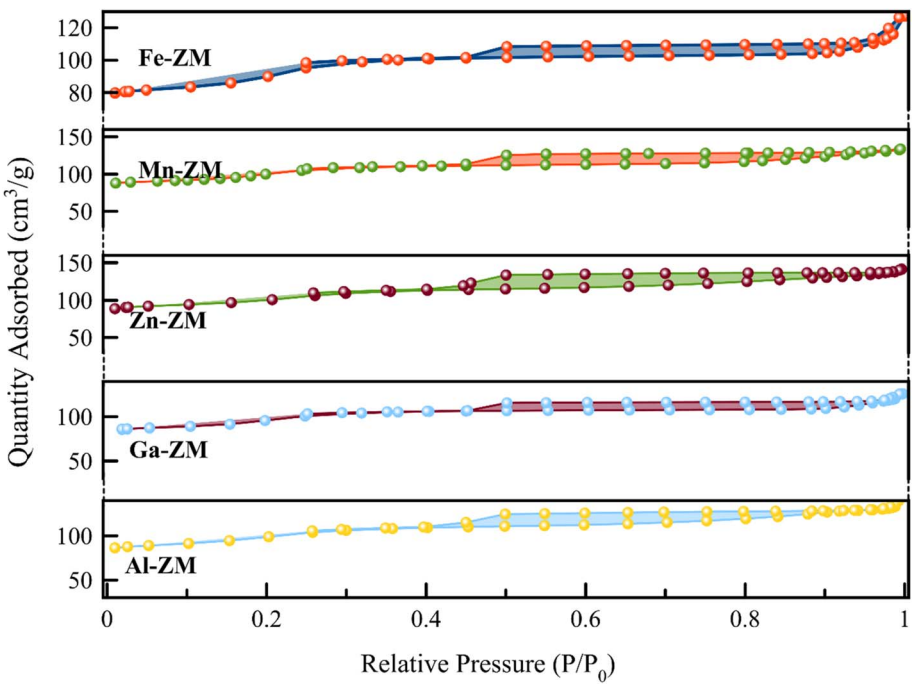

Fig. 4 N_2 adsorption–desorption isotherms of samples.

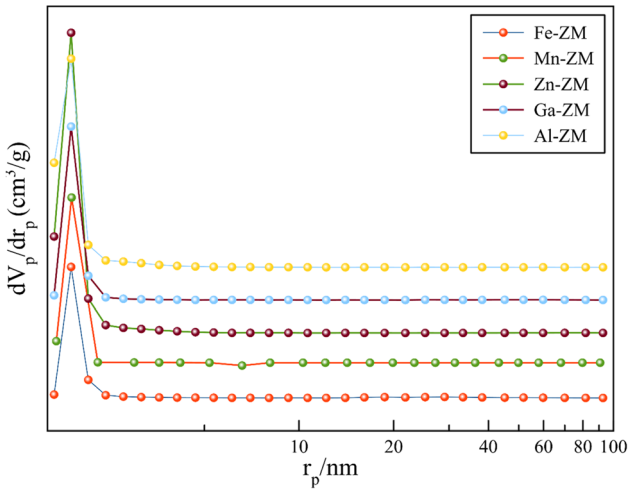

Fig. 5 Pore size distribution curves.

Table 1 Textural properties of incorporated zeolites

Catalyst	S_{BET} [a]	S_{ext} [b]	S_{ext}/S_{BET}	V_t [c]	V_{mic} [d]	V_{mes} [e]	d [f]
Fe-ZM	340	200	0.59	0.18	0.06	0.12	2.17
Zn-ZM	385	250	0.65	0.21	0.06	0.15	2.23
Al-ZM	364	251	0.69	0.22	0.06	0.16	2.37
Mn-ZM	340	197	0.58	0.20	0.07	0.13	2.38
Ga-ZM	361	220	0.61	0.19	0.05	0.14	2.10

[a] The specific surface area ($m^2\ g^{-1}$). [b] The external surface area ($m^2\ g^{-1}$). [c] The total pore volume ($cm^3\ g^{-1}$). [d] The micropore volume ($cm^3\ g^{-1}$). [e] The mesopore volume ($cm^3\ g^{-1}$). [f] The average pore diameter (nm).

Fig. 6 shows the results of ammonia desorption analysis for the substituted samples. The investigate of NH_3-TPD data showed that the incorporation of Mn and Ga metals had no effect on the total number of acid sites. However, the presence of Zn in the structure of the synthesized catalysts caused a slight increase in the number of available sites. This phenomenon was probably due to the reaction of Zn with the structural Al and the enhancement of the formation of internal acid sites and partial extra-structural species. According to Table 2, the decrease of the acid strength in both weak and strong acid sites was observed in all substituted samples with different metals because the peaks of weak and strong acid sites, in the temperature range of 150–250 °C and 375–500 °C, respectively, shifted to lower temperatures. Mn-ZM and Fe-ZM showed a more severe peak displacement in the area corresponding to the weak acid sites, due to the severe attenuation of these active sites, which play the major role in the production of light olefins.

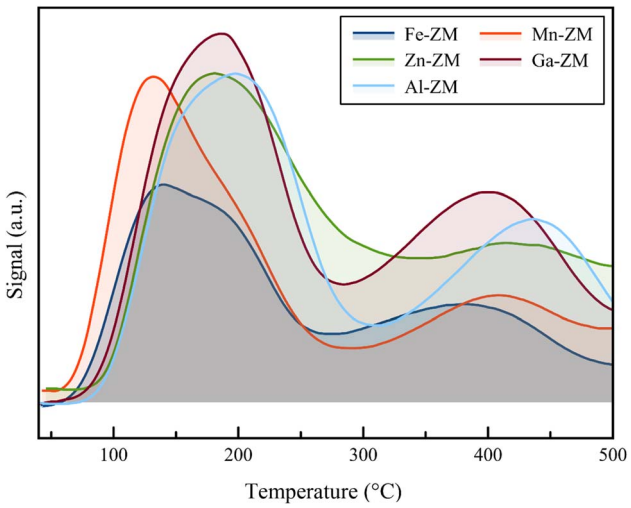

Fig. 6 NH_3-TPD plots of synthesized H-ZSM-5 catalysts.

H_2-TPR analysis (Fig. 7) of Ga-ZM and Fe-ZM showed that the synthetic samples lacked extra-structural species because no indicator peak was observed in the range of iron and gallium oxides. Therefore, in confirming the XRD and SEM results, it can be concluded that almost all metals were incorporated in the tetrahedral structure of synthetic zeolites, which results in minimizing the number of Lewis acid sites.

FT-IR analysis (Fig. 8) was used to identify the structural vibrations, relative intensities of Brønsted and Lewis acid sites, and surface silanol groups of the synthesized samples. FT-IR spectra of incorporated zeolites were taken in the range of 400–4000 cm^{-1}. Characteristic peaks of MFI structure were observed for all catalytic samples. The spectra in the wavelengths of 450, 550, 800, 1080 and 1250 cm^{-1} express the vibrations of the Si–O and Al–O bonds in the internal quadrilateral units of the SiO_4 and AlO_4, the vibrations within the networks of dual five-membered rings in the intermittent and repetitive structure of MFI, symmetric tensions of external bonds, the internal asymmetric tensile vibrations of Si–O–Si and Si–O–Al bonds and the vibrations of four branched five-membered rings in MFI structure, respectively. A very weak signal was seen in the range of 3650 to 3800 cm^{-1} for all samples. This signal indicates the vibrations of the O–H bond in can be assign to the Si–OH–Al groups (Brønsted acid sites, 3600 cm^{-1}), extra-framework Al–OH groups (3660 cm^{-1}), and internal and external silanol sites (3700–3750 cm^{-1}), respectively. Moreover, the low intensity of peak is the confirmation of low amount of Brønsted acid sites in the structure of incorporated zeolites.[36–39]

UV-vis analysis (Fig. 9) examines the coordination states of zeolites which indicates whether oxidation of metal ions is located in zeolite structure or not? UV-visible analysis of Fe-ZM sample showed the absorption range of 190 to 1100 nm. The specific peak of Fe-ZM (230 nm) was seen clearly which is related to the charge transferring from oxygen to Fe and it can be concluded that Fe ions exist in the tetrahedral coordination structure of inner framework of zeolite.[40]

3.2. Catalytic cracking performance

The investigation of the performance of the incorporated zeolites in the catalytic cracking of hexane to olefin (HTO) showed significant differences in the activity and selectivity of the synthetic samples. Considering the fact that this process

Table 2 Concentration of weak and strong acid site according to NH_3-TPD

Catalyst	Total acid (mmol g^{-1} ×10)	Weak acid (mmol g^{-1} ×10)	Strong acid (mmol g^{-1} ×10)	T_W[a] (°C)	T_S[b] (°C)	W/S	Si/M[c]
Fe-ZM	0.41	0.29	0.12	140	380	2.41	385
Zn-ZM	0.70	0.54	0.16	180	420	3.37	379
Al-ZM	0.63	0.42	0.21	197	437	2.00	391
Mn-ZM	0.65	0.52	0.13	133	408	4.00	386
Ga-ZM	0.63	0.42	0.21	188	400	2.00	391

[a] The temperature related to weak acidity zone. [b] The temperature related to strong acidity zone. [c] Obtained from ICP-OES.

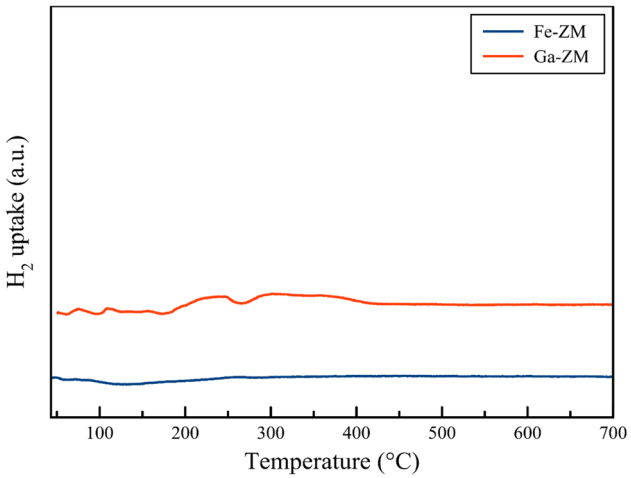

Fig. 7 H_2-TPR curves of Fe-ZM and Ga-ZM.

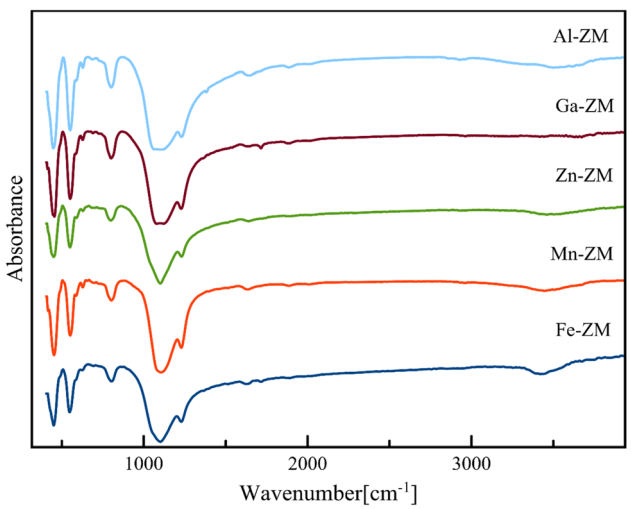

Fig. 8 FT-IR spectra of incorporated zeolites.

was performed in $WHSV_{HTO} = 25$, which was much higher than the conventional amounts in fixed- and fluidized-bed reactors (lab scale), their high performance in 10 h was remarkable. There was no sign of deactivation and coke deposition in the samples because the selectivity of light olefins as well as catalytic activity did not decrease significantly, mainly due to the role of the modifications performed and micro-meso-macroporous system in improving the transfer phenomena, which prevents the formation of coke precursors (BTX) by quickly removing the intermediates and products from catalytic bed (Fig. 10). According to the Zn-ZM sample, the role of the micro-meso-macroporous system can be confirmed because heavy products, even BTX, do not lead to side reactions and blockage of the mesopores, as the main sites in the transfer of intermediates and products by rapidly exiting the catalytic bed. The high activity (100%) as well as high selectivity of BTX compared to other samples indicated the presence of minor extra-structural species in this sample because H_2-TPR analysis showed that the low amount of substituted metals and modifications minimized the presence of extra-structural species. Partial extra-structural species, as Lewis acid sites, enhanced the production of aromatics by promoting hexane dehydrogenation.

According to Tables 2 and 3, Al-ZM produced the highest *P*/*E* ratio in HTO, which showed that strong and weak acid sites played the most important role in increasing the production of propylene in the catalytic cracking processes. Total olefin yield (TOY) and the selectivity of light olefins in Fe-ZM from the 6th hour of reaction onwards showed a clear decrease, indicating the blockage of some acid sites. In fact, Fe forms moderate acid sites, which enhance the production of propylene but limit the

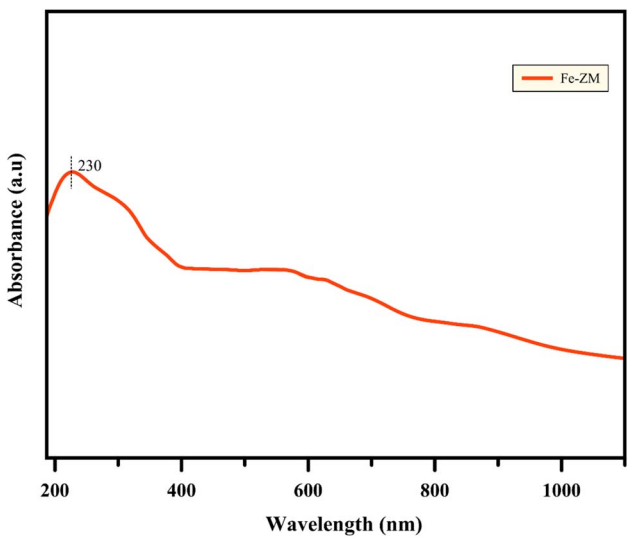

Fig. 9 UV-visible diffuse reflectance spectrum (DRS).

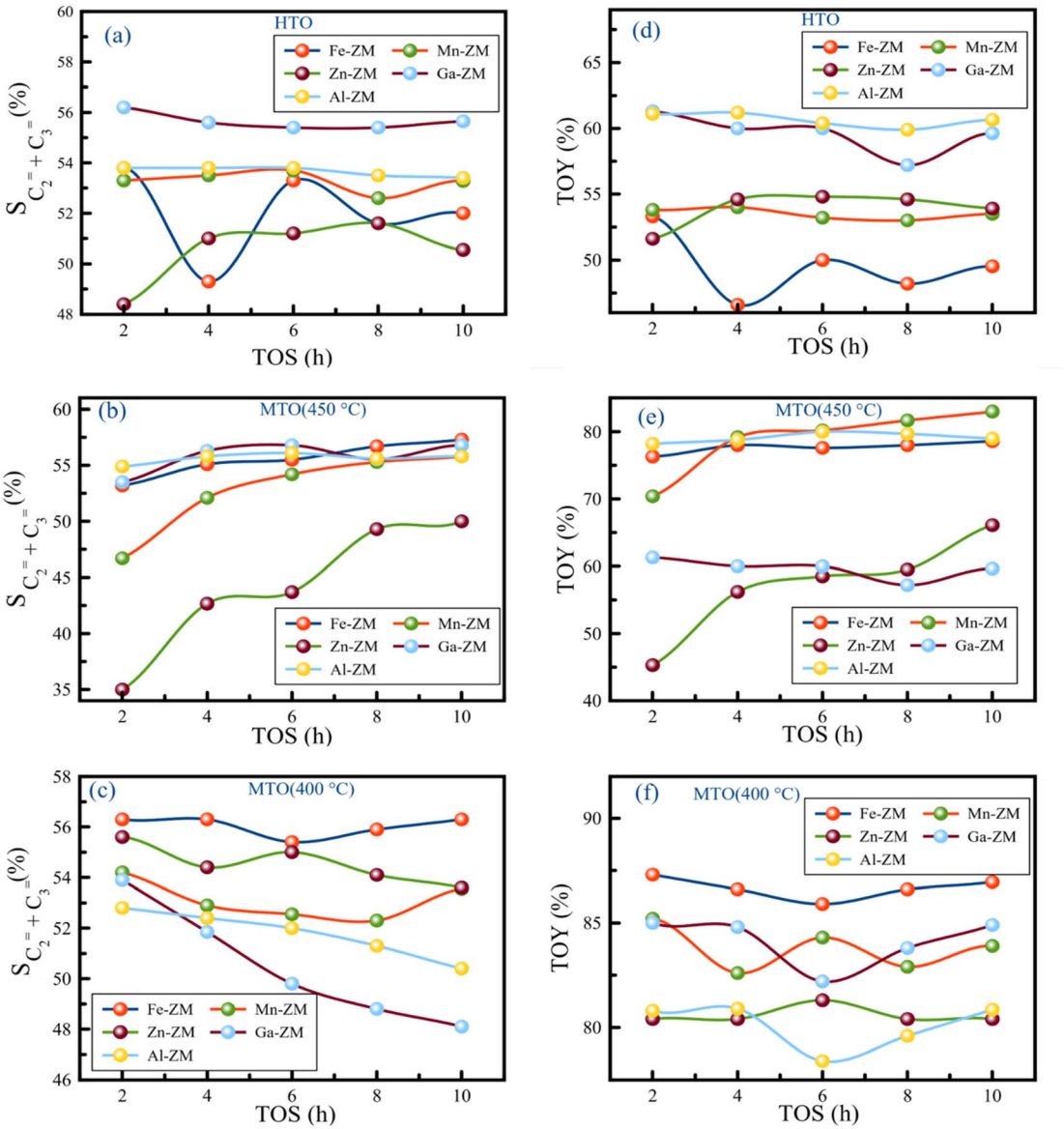

Fig. 10 TOS distribution of incorporated zeolites ($WHSV_{MTO}$ = 30 h^{-1} and $WHSV_{HTO}$ = 25 h^{-1}).

production of other olefins,[41,42] as evidenced by the high *P*/*E* ratio of Fe-ZM after Al-ZM. The highest TOY was also related to Al-ZM and Ga-ZM samples (Fig. 11). Therefore, to increase the production of propylene in the cracking processes in high WHSV using a green and sustainable catalyst, Al-ZM was introduced, which had the highest *P*/*E* ratio and TOY.

3.3. Methanol to olefins performance

For the first time, MTO process was carried out in microchannels with high feed flow, which showed impressive results. All samples showed acceptable stability with activity nearly 100% methanol conversion in a 10 h reaction at 400 and 450 °C, which can be definitely much higher in microchannels due to their inherent properties. The catalytic activity of the samples showed that the micro-meso-macroporous system consisting of microchannels and hierarchical nanocrystals (synthesized without additional template) in this process also improved the transfer phenomena and increased the activity of the incorporated catalysts.

The investigation of the performance of the samples at 450 °C showed that over time, the selectivity of light olefins and TOY increased, which was the most obvious in Zn-ZM. Considering the performance of this sample in HTO and the presence of minor extra-structural species, this species facilitated the conversion of methanol to olefins over time by strengthening the olefin-based cycle. However, the lower ratio of *P*/*E* in comparison with other samples showed that much more ethylene was produced which confirmed the results of HTO. Indeed, the more production of ethylene and arenes is a sign of the dominance arene based cycle in MTO.[43–45] Therefore, in the micro-meso-macroporous system, by preventing over reactions in MTO, the production of aromatics (which was significant in HTO) was

Table 3 Product distribution of incorporated samples in MTO and HTO processes after 10 hours

		Conv. (%)	$S_{(Alkanes)}$ (%)	$S_{(C_2^=)}$ (%) & $S_{(C_3^=)}$ (%)	$S_{(C_{4+}^=)}$ (%)	$S_{(BTX)}$ (%)	TOY (%)	*P*/*E*
HTO	Fe-ZM	88.8	24	16.25, 35.75	6.2	17.8	49.6	2.2
	Mn-ZM	81.8	29.3	17.76, 35.54	12.2	5.2	53.6	2
	Zn-ZM	100	18	18.74, 31.86	3.9	27.4	54.5	1.7
	Ga-ZM	90.5	27.8	17.96, 37.73	10.4	6.2	59.8	2.1
	Al-ZM	87.9	30.2	14.91, 38.78	15.3	0.9	60.6	2.6
MTO (450 °C)	Fe-ZM	100	22.2	5.50, 50.1	22.6	<0.1	78.2	9.1
	Mn-ZM	100	22.3	4.71, 48	25.6	<0.1	78.4	10.2
	Zn-ZM	100	39.2	10.5, 33.6	13.9	4.3	58	3.2
	Ga-ZM	100	16.9	9.78, 46.01	27.1	0.5	82.9	4.7
	Al-ZM	100	20.3	13.23, 42.36	23.5	0.6	79.1	3.2
MTO (400 °C)	Fe-ZM	100	13	4.59, 51.4	30.8	<0.1	86.8	11.2
	Mn-ZM	100	15.3	4.91, 48.18	30.5	0.2	83.6	9.8
	Zn-ZM	100	16.2	11.59, 42.9	25.5	3.3	80	3.7
	Ga-ZM	100	14.7	0, 50.5	33.2	0.3	83.7	∞
	Al-ZM	100	18.6	11.02, 40.77	28.6	0.6	80.4	3.7

limited, and instead ethylene was produced. On the other hand, the reduction of temperature in the study of Zn-ZM showed that from the 6th hour onwards, TOY and the selectivity of light olefins decreased, which is a sign of the obstruction of active acid sites in the production of light olefins. Reducing the temperature in the MTO also lead to the strengthening of the arene based cycle, which in general leads to the production of aromatics (as the precursors of coke formation) and ethylene, and thus the beginning of mesoporous occlusion. The dramatic increase of TOY at 400 °C compared to 450 °C (80% *vs.* 58%) also proved the claim of strengthening the arene based cycle. In fact, lowering the temperature had the highest impact on the increasing of TOY and the selectivity of light olefins. The high production of alkanes in Zn-ZM seemed to be due to the presence of Lewis acid sites, which convert more ethylenic and aromatic intermediates to alkanes by enhancing the elimination of hydrogen from the system. The decreasing of reaction temperature in all samples increased TOY and the selectivity of light olefins, which indicated the tremendous effect of micro-meso-macroporous system in removing the products as quickly as possible, because more aromatic intermediates are produced, which turn into aromatics if the reaction continues, with the

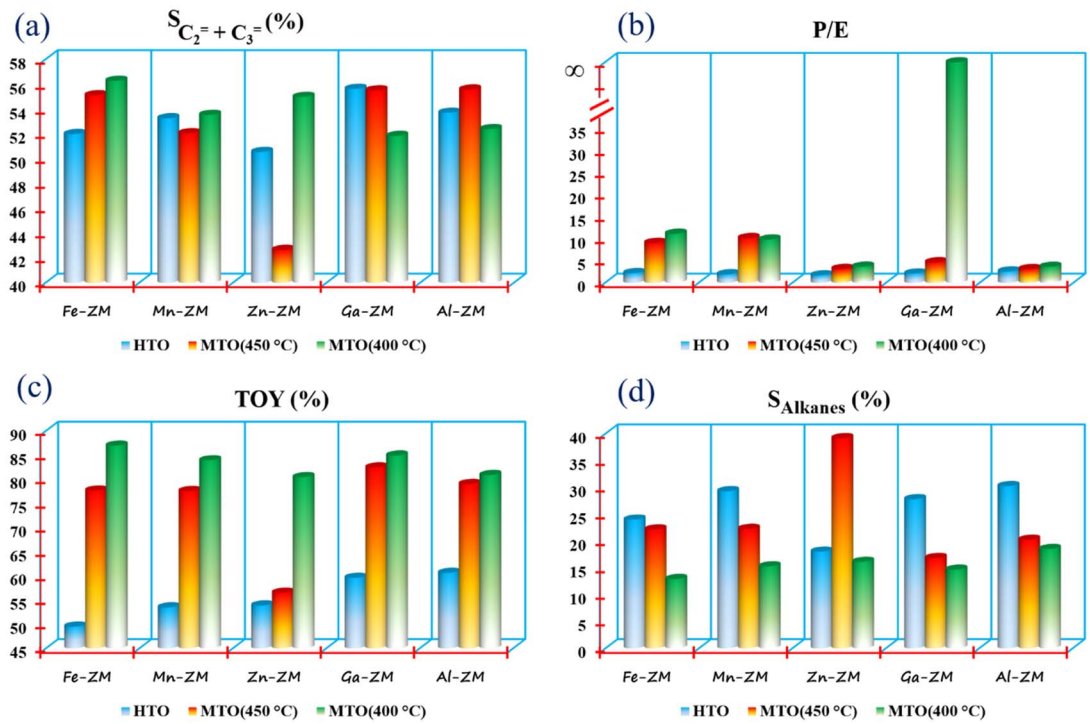

Fig. 11 *P*/*E* ratio, TOY, and selectivity of Alkanes and Light Olefins in HTO and MTO.

decrease of temperature and energy in the catalytic bed. However, the rapid exit and moderate acidity of samples lead to the production of olefins. All samples, except Mn-ZM, showed increased P/E ratio by decreasing the temperature, probably due to the greater conversion of aromatic intermediates to propylene. At 400 °C in Al-ZM and Ga-ZM, the passage of reaction time reduced the selectivity of light olefins, but the impressive performance of Ga-ZM showed that the longer the reaction time, the more propylene was produced, which reached $P/E \simeq \infty$ at 10th hour. In addition, TOY in these two samples did not obviously change during 10 hours. In MTO, Ga-ZM was introduced to produce more propene at 400 °C using a system that has the ability to run at high flow rates. The low production BTX in all samples also confirm rapid exit of products in this system.

3.4. Reactor productivity and catalyst consumption

Table 4 indicates the RP of the incorporated catalysts in the first 2 hours as well as the CC for HTO in microchannels and fixed-bed reactor. Due to the small amount of CO_2, CO and H_2 in the catalytic cracking processes at high temperatures, their amount has been disregarded in the calculations. All samples showed RP >3 for propylene as the preferred primary product, which is much higher than the ideal value (>0.5) based on sustainable metrics. The calculation of RP for the Al-ZM in the fixed-bed reactor, which was investigated in the previous study, showed that the RP for propylene was 0.06, which was even lower than the minimum required value for sustainable catalysis. Given the fact that the scaling-up of microchannels can be achieved by increasing the number of channels, which is called numbering-up, the significance of using microchannels on the industrial scales is inevitable.[46–48] Indeed, the reactor performance of synthesized catalysts has been investigated on a laboratory scale, and similar performance in higher scales can be achieved with the numbering-up.

The calculation of CC in 10 h showed that in order to achieve the ideal value of sustainable catalysis, at least Al-ZM must show 1180 h of stability in order to be introduced as an environmentally friendly catalyst. By contrast, the required stability for the same catalyst in the fixed-bed reactor is approximately 11 300 h.

Table 4 Calculated reactor productivity and catalyst consumption for incorporated zeolites (10th hour)

	Reactor productivity ideal value (>0.5)			Catalyst consumption ideal value (0.1>)	
Catalyst sample	P	$P+E$	∑olefins	Propylene	RH[a]
Ga-ZM_{Micro}	4	5.3	7	12.6	1260
Fe-ZM_{Micro}	3.3	4.3	5.6	15.1	1510
Mn-ZM_{Micro}	3.1	4.3	6	15.9	1590
Zn-ZM_{Micro}	3.2	4.5	5	15.7	1570
Al-ZM_{Micro}	4.2	5.3	7.9	11.8	1180
Al-$ZM_{Fixed\text{-}bed}$[32]	0.06	0.07	0.11	11.3	11 300

[a] Required stability hours to observe ideal value for the catalyst consumption.[13]

4. Conclusions

The investigation of the performance of the incorporated zeolites in HTO using microchannels showed that modern reactors have the ability to significantly increase RP and decrease CC compared to fixed-bed reactors. In fact, the importance of using microchannels, due to the much easier scale-up with a slight decrease in efficiency by numbering up method, becomes more valuable. Microchannels showed promising results in C–C coupling and cracking processes, which is also in line with green and sustainable chemistry approaches. The micro-meso-macroporous system using hierarchical multifunctional catalysts and microchannels, which can be implemented in several processes, clearly showed its importance. A group of synthetic catalysts can be used according to the desired product:

Al-ZM: for the purpose of propene and olefin production in HTO

Ga-ZM: for the purpose of propene production at 400 °C, and olefin production at 450 °C in MTO

Mn-ZM: for the purpose of propene production at 450 °C in MTO

Fe-ZM: for the purpose of olefin production at 400 °C in MTO

Conflicts of interest

There are no conflicts to declare.

References

1 I. Yarulina, A. D. Chowdhury, F. Meirer, B. M. Weckhuysen and J. Gascon, *Nat. Catal.*, 2018, **1**, 398–411.
2 N. C. Shiba, X. Liu and Y. Yao, *Fuel Process. Technol.*, 2022, **28**, 107489.
3 A. Portillo, A. Ateka, J. Ereña, J. Bilbao and A. T. Aguayo, *Fuel Process. Technol.*, 2022, **238**, 107513.
4 L. Lin, A. M. Sheveleva, I. da Silva, C. M. A. Parlett, Z. Tang, Y. Liu, M. Fan, X. Han, J. H. Carter, F. Tuna, E. J. L. McInnes, Y. Cheng, L. L. Daemen, S. Rudić, A. J. Ramirez-Cuesta, C. C. Tang and S. Yang, *Nat. Mater.*, 2020, **19**, 86–93.
5 S. Bailleul, I. Yarulina, A. E. J. Hoffman, A. Dokania, E. Abou-Hamad, A. D. Chowdhury, G. Pieters, J. Hajek, K. De Wispelaere, M. Waroquier, J. Gascon and V. Van Speybroeck, *J. Am. Chem. Soc.*, 2019, **141**, 14823–14842.
6 I. Yarulina, K. De Wispelaere, S. Bailleul, J. Goetze, M. Radersma, E. Abou-Hamad, I. Vollmer, M. Goesten, B. Mezari, E. J. M. Hensen, J. S. Martínez-Espín, M. Morten, S. Mitchell, J. Perez-Ramirez, - U. Olsbye, B. M. Weckhuysen, V. Van Speybroeck, F. Kapteijn and J. Gascon, *Nat. Chem.*, 2018, **10**, 804–812.
7 J. Towfighi, H. Zimmermann, R. Karimzadeh and M. M. Akbarnejad, *Ind. Eng. Chem. Res.*, 2002, **41**, 1419–1424.
8 V. Blay, B. Louis, R. Miravalles, T. Yokoi, K. A. Peccatiello, M. Clough and B. Yilmaz, *ACS Catal.*, 2017, **7**, 6542–6566.
9 C. Li, C. Paris, J. Martínez-Triguero, M. Boronat, M. Moliner and A. Corma, *Nat. Catal.*, 2018, **1**, 547–554.

10 R. A. Sheldon, *Green Chem.*, 2017, **19**, 18–43.
11 J. B. Zimmerman, P. T. Anastas, H. C. Erythropel and W. Leitner, *Science*, 2020, **367**, 397–400.
12 F. Alpizar, T. Backhaus, N. Decker, I. Eilks, N. Escobar-Pemberthy, P. Fantke, K. Geiser, M. Ivanova, O. Jolliet, H.-S. Kim, K. Khisa, H. Gundimeda, D. Slunge, S. Stec, J. Tickner, D. Tyrer, N. Urho, R. Visser, M. Yarto, V. G. Zuin, B. Alo, V. Barrantes, A. Makarova, Y. Chen, M. Abdelraouf and N. Suzuki, *UN Environment Global Chemicals Outlook II-From Legacies to Innovative Solutions: Implementing the 2030 Agenda for Sustainable Development*, 2019.
13 J.-P. Lange, *Nat. Catal.*, 2021, **4**, 186–192.
14 P. T. Anastas and J. B. Zimmerman, *Green Chem.*, 2019, **21**, 6545–6566.
15 A. Agarwal, D. Sengupta and M. El-Halwagi, *ACS Sustainable Chem. Eng.*, 2018, **6**, 2407–2421.
16 Y. Ji, H. Yang and W. Yan, *Catalysts*, 2017, **7**, 367.
17 S. Mintova, M. Jaber and V. Valtchev, *Chem. Soc. Rev.*, 2015, **44**, 7207–7233.
18 E. M. Gallego, M. T. Portilla, C. Paris, A. León-Escamilla, M. Boronat, M. Moliner and A. Corma, *Science*, 2017, **355**, 1051–1054.
19 X. Liu, J. Shi, G. Yang, J. Zhou, C. Wang, J. Teng, Y. Wang and Z. Xie, *Commun. Chem.*, 2021, **4**, 1–10.
20 F. Chen, J. Hao, Y. Yu, D. Cheng and X. Zhan, *Microporous Mesoporous Mater.*, 2022, **330**, 111575.
21 H. Sharbini Kamaluddin, X. Gong, P. Ma, K. Narasimharao, A. D. Chowdhury and M. Mokhtar, *Mater. Today Chem.*, 2022, **26**, 101061.
22 J. Shi, Y. Wang, W. Yang, Y. Tang and Z. Xie, *Chem. Soc. Rev.*, 2015, **44**, 8877–8903.
23 A. Primo and H. Garcia, Zeolites as catalysts in oil refining, *Chem. Soc. Rev.*, 2014, **43**, 7548–7561.
24 W. Dai, L. Yang, C. Wang, X. Wang, G. Wu, N. Guan, U. Obenaus, M. Hunger and L. Li, *ACS Catal.*, 2018, **8**, 1352–1362.
25 Y. Wang, T. Yokoi and T. Tatsumi, *Microporous Mesoporous Mater.*, 2022, **19**, 112353.
26 G. Kolb and V. Hessel, *Chem. Eng. J.*, 2004, **98**, 1–38.
27 Y. He, S. Guo, K. Chen, S. Li, L. Zhang and S. Yin, *ACS Sustainable Chem. Eng.*, 2019, **7**, 17616–17626.
28 J. Lerou, A. Tonkovich, L. Silva, S. Perry and J. McDaniel, *Chem. Eng. Sci.*, 2010, **65**, 380–385.
29 J. Chen and T. Li, *Energy Fuels*, 2019, **33**, 12026–12040.
30 X. Hou, Y. S. Zhang, G. T. Santiago, M. M. Alvarez, J. Ribas, S. J. Jonas, P. S. Weiss, A. M. Andrews, J. Aizenberg and A. Khademhosseini, *Nat. Rev. Mater.*, 2017, **2**, 1–15.
31 M. R. Sakha, S. Soltanali, D. Salari, M. Rashidzadeh and P. Halimitabrizi, *New J. Chem.*, 2021, **45**, 13833–13846.
32 M. R. Sakha, S. Soltanali, D. Salari, M. Rashidzadeh and P. H. Tabrizi, *J. Solid State Chem.*, 2021, **301**, 122342.
33 M. Thommes, K. Kaneko, A. V. Neimark, J. P. Olivier, F. Rodriguez-Reinoso, J. Rouquerol and K. S. W. Sing, *Pure Appl. Chem.*, 2015, **87**, 1051–1069.
34 S. Kim, G. Park, M. H. Woo, G. Kwak and S. K. Kim, *ACS Catal.*, 2019, **9**, 2880–2892.
35 H. Li, Y. Wang, C. Fan, C. Sun, X. Wang, C. Wang, X. Zhang and S. Wang, *Appl. Catal., A*, 2018, **551**, 34–48.
36 S. Wang, X. Lan, S. Xing, B. Ali and T. Wang, *React. Chem. Eng.*, 2022, **7**, 1555–1565.
37 A. A. Gabrienko, I. G. Danilova, S. S. Arzumanov, L. V. Pirutko, D. Freude and A. G. Stepanov, *J. Phys. Chem. C*, 2018, **122**, 25386–25395.
38 M. Grahn, A. Faisal, O. G. Öhrman, M. Zhou, M. Signorile, V. Crocellà, M. S. Nabavi and J. Hedlund, *Catal. Today*, 2020, **345**, 136–146.
39 J. Hedlund, M. Zhou, A. Faisal, O. G. Öhrman, V. Finelli, M. Signorile, V. Crocellà and M. Grahn, *J. Catal.*, 2022, **410**, 320–332.
40 R. P. Vélez, I. Ellmers, H. Huang, U. Bentrup, V. Schünemann, W. Grünert and A. Brückner, *J. Catal.*, 2014, **316**, 103–111.
41 X. Jiang, X. Su, X. Bai, Y. Li, L. Yang, K. Zhang, Y. Zhang, Y. Liu and W. Wu, *Microporous Mesoporous Mater.*, 2018, **263**, 243–250.
42 K. Bian, A. Zhang, H. Yang, B. Fan, S. Xu, X. Guo and C. Song, *Ind. Eng. Chem. Res.*, 2020, **59**, 22413–22421.
43 T. Liang, J. Chen, Z. Qin, J. Li, P. Wang, S. Wang, G. Wang, M. Dong, W. Fan and J. Wang, *ACS Catal.*, 2016, **6**, 7311–7325.
44 S. Müller, Y. Liu, F. M. Kirchberger, M. Tonigold, M. Sanchez-Sanchez and J. A. Lercher, *J. Am. Chem. Soc.*, 2016, **138**, 15994–16003.
45 Z. Wang, Z. Wang, L. A. O'Dell, X. Zeng, C. Liu, S. Zhao, W. Zhang, M. Gaborieau, Y. Jiang and J. Huang, *Angew. Chem., Int. Ed.*, 2019, **58**, 18061–18068.
46 P. Watts and C. Wiles, *Chem. Commun.*, 2007, **5**, 443–467.
47 M. Schoenitz, L. Grundemann, W. Augustin and S. Scholl, *Chem. Commun.*, 2015, **51**, 8213–8228.
48 Z. Dong, Z. Wen, F. Zhao, S. Kuhn and T. Noël, *Chem. Eng. Sci.: X*, 2021, **10**, 100097.